

Tidal Triggering of the Harmonic Noise in Ocean Bottom Seismometers

R. Reddy¹, P. Dewangan^{1*}, L. Arya¹, P. Singha¹ and K. A. Kamesh Raju¹

¹CSIR-National Institute of Oceanography, Dona Paula, Goa – India – 403004.

*Corresponding author Email: pdewangan@nio.org

Abstract

We observed a harmonic noise (HN) in DEPAS ocean bottom seismometers (OBSs) data recorded from the Andaman-Nicobar region. The HN is characterized by sharp spectral peaks with a fundamental frequency and several overtones occurring at integer multiples of the fundamental frequency. We used an automated algorithm to quantify the occurrence of HN for the entire four-month deployment period (1st January 2014 to 30th April 2014). The algorithm detected more than 23 days of HN for some OBS stations. The spectral analysis of the hourly count of HN shows distinct lunar and solar tidal periodicities at 4.14, 6.1, 6.22, 12, and 12.4 hr as well as 13.66 days. The observed periodicities provide evidence of tidal triggering of HN. The HN is generated by the strumming of head buoy due to seafloor currents initiated by oceanic tides in the Andaman-Nicobar region.

Key Points:

- Harmonic noise is observed in the DEPAS OBS due to strumming of head-buoy from tidal currents.
- The harmonic noise shows distinct energy peaks at lunar and solar tidal constituents: S2, M2, S4, M4, M6, Mf, MS4, 2MS2 and 2SM2.
- The strongest harmonic noise is observed during spring tides.

1. Introduction

A large number of earthquakes occur at plate boundaries under the oceans while global seismic stations are mainly distributed on land. The uneven coverage of global stations limits our understanding of the Earth's interior (Wyssession, 1996; Romanowicz, 1991). Therefore, there is a growing interest in the seismological community to record earthquake data beneath the oceans. Ocean-bottom seismometers (OBSs; Cox *et al.*, 1984; Webb and Crawford, 1999) and water column hydrophones (Simons *et al.*, 2009; Hello *et al.*, 2011; Fox and Dziak, 1998; Dziak and Fox, 1999) have great potential to record distant earthquakes and overcome the limitations caused by the inhomogeneous distribution of seismic observatories. However, processing and interpretation of OBS data have some significant challenges and technical difficulties.

Unlike continental station, OBS records distinct noises related to ocean waves, wind, and ocean currents (Webb, 1998). The primary microseismic or single frequency microseism noise (11-25 s) with a dominant period of 14 s is generated in shallow waters where the depth is less than the wavelength of wind-forced gravity waves (Bromirskiet *al.*, 2005). The secondary microseisms or double frequency (DF) microseism noise (1-10 s) with a dominant period of 7 s is generated by the nonlinear interaction of ocean waves traveling in opposite directions (Longuet-Higgins, 1950). The infragravity waves which are characterized by small wave height, long wavelength, and long-period (30-500 s) induce long period noise (> 30 s) on the vertical component of seismometer (Webb, 1998, 2007; Ardhuinet *al.*, 2015; Doran and Laske, 2016). The other noises recorded on OBS data are related to the uncontrolled deployment of OBS on the seafloor. For example, the ocean bottom currents acting on the OBS frame can tilt the instrument and induce tilt-noise (Duennebieret *al.*, 1987; Trehu, 1985; Webb, 1998; Crawford and Webb, 2000). Long period (20-60 s) tilt noise is more prominent on the horizontal components, whereas seismometer self-noise is dominant on the vertical component (Stähler, 2016). The gimbal system and data logger are other probable sources that could generate short period noise on all the components of OBS (Stähler, 2016).

Noise can also be locally generated by an OBS instrument due to its interaction with seafloor currents. A radio antenna or other elements such as taut cables attached to an OBS instrument are observed to strum due to the current movement, and strumming can produce a harmonic noise (HN) with a narrow and energetic peak at frequencies of few hertz (Webb, 1998). Such HN has been reported in a frequency range of 1-10 Hz from DEutscher Geräte-Pool für Amphibische Seismologie (DEPAS) OBSs deployed off the Baltic Sea (Stähler *et al.*, 2018). Such noise may be present in other experiments carried out with DEPAS OBS, for example, NEAREST project in the Gulf of Cadiz (Geissler *et al.*, 2009, 2010), EXUPERY project in the north Atlantic (Rios *et al.*, 2010), WACOM

project in the Amundsen Sea (Gohl, 2010) and DOCTAR project in the north Atlantic. HN is also reported from Scripps Institution of Oceanography (SIO) OBSs deployed off the Canary Islands (Ugalde et al. 2019). Chang et al. (2016) also observed similar HN in a frequency range of 2-4 Hz from the coast of southeast Taiwan. HN occurring in a narrow frequency range of 5.5-7.5 Hz is classified as “type 6” noise by Olofsson (2010). HN with a fundamental frequency of 6 Hz is quite common in OBS data, and a dedicated website (<http://www.obsip.org/data/6hz-noise/>) reports the occurrence of such HN from various cruises and experiments like the East Pacific Rise experiment (2003-2007), the Colza experiment (2007-2008), the Lau basin recovery cruise (2009), the ALEUT cruise (2011), the Juan de Fuca cruise (2012), the ENAM and Santorini experiments (2014-2015), the SEGMeNT/Malawi experiment (2015) and the 2018 Kilauea experiment. Pontoise and Hello (2002) also observed similar HN offshore Ecuador, but attributed it to methane seeps. In general, HN shows tidal periodicities and correlates with periods of strong ocean bottom currents (Duennebieer *et al.*, 1981). It is essential to understand the mechanism for the generation of such noise so that it may be minimized or removed from OBS data. The characterization of noise is also required for the selection of potential sites for permanent ocean floor observatories as well as for temporary deployments of OBS arrays (Wenz, 1962; Webb and Cox, 1986; Cox and Jacobs, 1989; D'Spainet *et al.*, 1991; Babcock *et al.*, 1994; Webb, 1998).

The data recorded from a passive OBS experiment in the Andaman-Nicobar subduction zone gave us an excellent opportunity to study various types of ocean-generated noise. The nature of the ambient noise and site response of the OBS stations were analyzed by Dewangan et al. (2017). In the present study, we report the occurrence of HN in the OBS data and attempt to explain its genesis in this region.

2. The passive seismic experiment in the Andaman-Nicobar region

The Andaman-Nicobar region is seismically active owing to the subduction of the Indo-Australian plate beneath the southeast Asian plate (Curry, 2005). We deployed twelve broadband DEPAS OBSs to study the geodynamic and tectonic processes of the region (Dewangan *et al.*, 2017; Singha *et al.*, 2019). The OBSs were deployed during the last week of December 2013 and retrieved during the first week of May 2014. Güralp CMG-40T seismometers with a corner period of 60 s and a sensitivity of 2000 V.s/m and broadband HTI-04-PCA/ULF hydrophones (100 s to 8 kHz) were used for the passive OBS experiment. In the present study, we analyze seismic waveform data from the nine OBSs that successfully recorded data. OBS01 and OBS12 were located on the Indian plate close to the trench (Fig. 1), OBS03 and OBS11 were located in the forearc basin and OBS02 was located off Nicobar Island, where submarine volcanism has been reported (Kamesh Raju *et al.*,

2012). This off Nicobar Island also witnessed the largest instrumentally recorded earthquake swarm triggered by the 26th December 2004 tsunamigenic earthquake (Lay *et al.*, 2005). OBS06 and OBS07 were situated on the Andaman back-arc spreading center (ABSC), while OBS05 and OBS09 were located on the Alcock and Sewell seamounts, respectively (Fig. 1).

3. Automatic detection of the harmonic noise

We used the automated algorithm proposed by Roman(2017) to detect and characterize the observed HN. The algorithm utilizes a fundamental frequency detection approach using the harmonics product spectrum to locate the HN and characterize their frequency content. The critical detection parameters used in the algorithm are chosen carefully to avoid false detection of noise. We used following parameters in the algorithm: minimum frequency of detection is 0.3 Hz, harmonic strength index (HSI) is greater than two, and minimum number of overtones is four. The HSI is defined as the ratio of the power of the signal at the fundamental or harmonic frequency to the power of the signal at interharmonic. The performance of the algorithm was manually checked, and it was found that the predicted occurrence of noise matched well with the visual observation.

4. Harmonic noise in the DEPAS OBS data

The main characteristic of HN is sharp spectral peaks (Fig. 2); therefore, we computed the spectrogram of the seismic data for all the nine stations from 1st January to 30th April 2014. The signal was divided into one-hour segments, and the spectrogram was computed for each segment using a sliding window of 10.24 s (equivalent to 1024 samples), with a 50% overlap. A one-hour raw record of the vertical, horizontal, and pressure components at OBS02 and their spectrogram illustrating the occurrence of HN are shown in Figure 2. The spectrograms reveal several sharp peaks which are characterized by a fundamental frequency and up to ten overtones occurring at integer multiples of the fundamental frequency. In general, the HN is more frequently observed on the spectrogram of vertical and horizontal components than on the pressure component. Low-frequency noise (< 1 Hz) is stronger on the pressure component.

5. Tidal modulation of the harmonic noise

An hourly count of HN estimated from the vertical components of the OBS stations is shown in Figure 3, and the total duration of HN for each station is listed in Table 1. HN is frequently observed at stations OBS01, OBS02, OBS09, and OBS11, while stations OBS05, OBS06, OBS07, and OBS12 show intermittent occurrence and OBS03 shows negligible occurrence of HN. Calculated HN durations are similar on the horizontal components but lower on the pressure component (Fig. 4). A broad, low-frequency fluctuation with a periodicity of ~15 days is observed,

superimposed by a high-frequency fluctuation with multiple periodicities ranging from 6 to 12 hr. In order to quantify the observed periodicities, we performed a Fast Fourier Transform (FFT) on the hourly count of HN for the stations with frequent occurrence of HN (OBS01, OBS02, OBS09, and OBS11). The FFT spectrums show several sharp peaks corresponding to solar and lunar tides (Fig. 5). The following tidal components (Andersen, 1999) are observed on most of the OBS stations: the two principal semi-diurnal constituents related to the moon and the sun, with periods of 12.42 hr (M2) and 12.00 hr (S2); the lunar fortnightly (Mf) tidal component with a period of 13.66 days (327.84 hr); the fourth and sixth lunar diurnals, which are overtones of M2 with periods of 6.21 hr (M4) and 4.14 hr (M6); and the compound tides due to the interaction of M2 and S2, with periods of 12.87 hr (2MS2), 11.60 hr (2SM2), and 6.10 hr (MS4). Diurnal constituents with periods of 23.93 hr (K1) and 25.81 hr (O1) are not observed in the present study. The oceanic tidal form number, defined as the ratio of the amplitudes of diurnal constituents to semi-diurnal constituents, is less than 0.2 in the Andaman-Nicobar region indicating that the tides are predominantly semidiurnal with negligible diurnal component (Murty and Henry, 1983). We observe similar tidal periodicities for the horizontals and pressure components.

6. The genesis of harmonic noise in DEPAS OBS

Harmonic signal is considered to be a subclass of volcanic tremor and is often observed as a precursor to major volcanic eruptions (Konstantinou and Schlindwein, 2002). In the present study, we observed the harmonic signal for many OBSs located in diverse geological environments like the forearc basin (OBS11), the Indian plate in the Bay of Bengal (OBS01 and OBS 12), the Andaman backarc spreading center (OBS06 and OBS07) which are far away from any known volcanic sources. Therefore, the observed harmonic is possibly not related to volcanic tremor. Other known sources of noise like air guns, ship propellers (fishing boats, tankers), large mammals (e.g., whales), T-waves (Olofsson, 2010; Franek *et al.*, 2014), and ocean waves, wind, and surface currents (Webb, 1998) are unlikely as they cannot explain the continued occurrence of harmonic signal with tidal periodicities. However, the movement of tidal currents through and around the instrument package may induce noise with tidal periodicities (Thomson *et al.*, 1990; Tolstoy *et al.*, 1998; Crawford and Webb, 2000). At short periods, such noises are generated by shedding of Karman vortices from antennas and other resonant obstructions (Duennebieer *et al.*, 1981). At long periods, tilting of the OBS package by bottom currents can generate strong noise on the horizontal components (Crawford and Webb, 2000). It is likely that the HN observed in the present study is related to seafloor currents generated by tides.

In the DEPAS OBS, a head buoy with positive buoyancy is tied to the instrument package with a 10 m rope for easy retrieval (Fig. 6a). The rope comes into tension on deployment (Fig. 6b), and the flow of ocean currents around the obstacle leads to Karman vortex shedding. The currents cause the tensioned cable to strum, thereby generating the HN (Stähler *et al.*, 2018). As shown by Stähler *et al.* (2018), the fundamental frequency for head buoy generated HN is around 0.48 Hz for a standard DEPAS OBS package. The vortex shedding frequency (f_{vort}) varies linearly with current velocity (v) as,

$$f_{vort} = 10.5 \times v . \quad (\text{eq. 1})$$

If the shedding frequency is close to the fundamental frequency of the cable or one of its overtones, the resonance phenomenon will generate a strong HN even for a moderate current velocity. The fundamental frequency observed in the present study is close to 0.48 Hz or integer multiples of 0.48 Hz, which matches well with that predicted from the model. Therefore, the HN originates due to the strumming of the head buoy by bottom currents. The HN shows tidal periodicities, indicating that the bottom currents are governed by tidal forces. Further, the HN is absent in a nearby land station (HUTB), confirming that the noise is generated by the OBS instrument while deployed in the ocean. In the present experiment, HN is observed at the stations located in deep waters (> 1500 m) which give an opportunity to study the mechanism of generation of HN in the open ocean.

7. Association of harmonic noise with internal tides in the Andaman-Nicobar region

While the HN is observed at all the stations, the total duration of HN varies greatly among stations from 4.7 to 544 hrs. In general, the OBSs located in water depths greater than 3400 m (OBS03, OBS06, OBS07 and OBS12) show limited occurrence of HN (< 30 hr), while those located in depths shallower than 2300 m (OBS02, OBS09 and OBS11) show sustained occurrence of HN (> 250 hr). We attempt to explain the spatial distribution of HN by predicting the seafloor currents in the Andaman-Nicobar region.

Seafloor currents with tidal periodicities occur due to rise and fall of sea level by astronomical tides. The movement of seawater generates surface tidal currents in coastal shelf regions, but such currents are expected to be weak in the open ocean and might not fully explain the observed HN as the OBSs are all located in relatively deep waters (> 1500 m). Strong bottom currents are also observed in deep waters along submarine canyons and continental slope regions due to internal tides (Cacchione and Drake, 1986; Dickson and McCave, 1986; Cacchione *et al.*, 2002; Puiget *et al.*, 2004; Quaresma *et al.*, 2007). Internal tides are gravity waves analogous to surface wave, but travels in the interior of the ocean and show tidal periodicities (Munk, 1981; Hendershott, 1981).

The internal tides are characterized by perturbation in the depth of the pycnocline (an interface of different densities) and strong subsurface currents. Bottom currents up to 30 m/s associated with internal tides are reported from water depths ranging from 46 to 4200 m in various submarine canyons and sea valleys (Shepard *et al.*, 1979). Such currents are also reported from the continental slopes of the Atlantic margin (McGregor, 1979), northern California and New Jersey (Cacchione *et al.*, 2002), northwestern Alboran (Puig *et al.*, 2004), offshore Portugal (Quaresma *et al.*, 2007), offshore Israeli (Reiche *et al.*, 2018), and the South China Sea (Xie *et al.*, 2018) indicating the widespread presence of bottom currents in the open ocean (Pomar *et al.*, 2012). In density-stratified water column, the energy of internal tides propagates at an angle defined by the tidal frequency, latitude, and density gradient (Pingree and New, 1991). If the propagation angle is close to the bathymetry slope, the internal energy is trapped along the bottom and generates strong currents (Cacchione *et al.*, 2002; Cacchione and Pratson, 2004). Such currents often govern the dip of the continental slope (Cacchione *et al.*, 2002). We now explore the presence of internal tides in the Andaman-Nicobar region.

Internal tides are generated by strong oceanic tides, a stratified water column and irregular ocean floor topography such as shelf breaks, sills or seamounts with steep slopes (Apel, 2002). The Andaman Sea meets all the conditions for the generation of strong internal tides: an irregular bottom topography with steep slopes related to the accretionary prism/seamounts/volcanoes, an intense vertical stratification (Sarma and Narvekar, 2001), and strong tides. In fact, Perry and Schimke (1965) was the first to report the presence of internal waves in the Andaman Sea based on oceanographic measurements. Later, Osborne and Burch (1980) carried out a systematic study in the Andaman Sea using a current-meter and showed that the shallow water regions off northern Sumatra and the Nicobar Islands are favorable locations for the generation of internal tides. Internal tides in the Andaman Sea show tidal periodicities of 12.42 hr and are highly energetic during spring tides (Osborne and Burch, 1980; Hyder *et al.*, 2005). Internal solitary waves generated due to internal tides can be observed in optical / synthetic aperture radar (SAR) images as they create a rough sea-surface due to convergence and divergence of the horizontal currents. Extraordinary large amplitude, internal tides originating from the banks of the Andaman-Nicobar Islands were observed in the SAR images from the Andaman Sea (Alpers *et al.*, 1997). In the present study, we have analyzed the MODIS (Moderate Resolution Imaging Spectroradiometer) reflectance imagery data from Terra and Aqua satellites (<https://worldview.earthdata.nasa.gov/>) during the OBS deployment period and observed the signature of internal tides (sea-surface roughness) in the Andaman region (Fig. 7a). The internal tides are preferentially generated in shallow waters near the Sombrero channel (northern

Sumatra), between the Car Nicobar and the Nicobar Islands, and in the Prepara channel (north of Andaman Islands). The analysis of internal waves in the Andaman Sea using the Massachusetts Institute of Technology general circulation model (MITgcm) also indicate that the internal tides are generated near the Sombrero channel, Prepara channel, and south of the Car Nicobar Island due to the presence of irregular and steep topography (Fig. 7b modified after Mohanty *et al.*, 2018). After generation, the internal tides travel along the local bathymetry in the Andaman-Nicobar region (da Silva and Magalhaes, 2016) and may generate strong seafloor currents. Interestingly, the OBSs that are located close to the generation sites i.e., OBS01, OBS02, and OBS11 show enhanced HN where energy flux is large (Mohanty *et al.*, 2018). OBS03 is an exception as it was located inside the depression created by the fault system and was probably unaffected by bottom currents. The HN is also strong at OBS09 located on the Alcock seamount, and seamounts can generate internal tides (Holloway and Merrifield, 1999). We expected the HN to be stronger on OBS05 located on the Sewell seamount, but higher ambient noise observed in OBS05 in the frequency range of 1 to 10 Hz (Dewangan *et al.*, 2017) might have hampered the identification of HN. The OBSs located in deeper waters (> 3400 m) and away from the generation sites, i.e., OBS06, OBS07, and OBS12 show limited occurrence of HN. Thus, the spatial distribution of HN can be explained by the generation and propagation of internal tides in the Andaman-Nicobar region. Similar tremor like signals due to internal tides are also reported in the OBS data off the coast of southeast Taiwan (Chang *et al.*, 2016).

The internal tides in the Andaman region were observed in MODIS images: during spring tides around 4th Feb, 3rd March, 19th March, 30th March, 16th April and 29th April 2019 . In order to explain the temporal distribution of HN, we compare the observed HN with the predicted barotropic (surface) tidal currents at OBS02 and OBS09. The tidal currents were computed using TPXO 9.1 model for global ocean tides (Egbert and Erofeeva, 2002) via TPXO web service (<https://tpxows.azurewebsites.net/> accessed on 11th Nov 2019). A visual comparison between the daily count of the HN estimated at OBS02 and the peak envelop of the total tidal current shows that the enhanced HN occurs during strong tidal currents near spring tides, and HN is almost negligible during weak tidal currents near neap tides (Fig. 8a). Similar relationship is also observed at OBS09 (Fig. 8b) indicating that the observed HN is also linked to barotropic tidal currents in the Andaman-Nicobar region. In order to understand the relative contribution of the surface and internal tides, a systematic study of bottom currents is warranted in the Andaman-Nicobar region.

8. Conclusions

Harmonic noise (HN) is observed at all OBS stations spread over a diverse geological environment in the Andaman-Nicobar region. The major characteristics of the HN are listed below:

- 1) The spectrogram of the HN shows sharp spectral peaks which are characterized by a fundamental frequency with several overtones occurring at integer multiples of the fundamental frequency.
- 2) HN is generated in DEPAS OBS due to the interaction of tidal currents with the rope attached to OBS instrument (Stähler et al., 2018).
- 3) A spectral analysis of the hourly count of HN shows distinct peaks occurring at the lunar and solar tidal periodicities, providing evidence of tidal triggering.
- 4) The spatial distribution of HN is strongly linked to predicted strengths of barotropic tidal currents. Stations located in the vicinity of Car Nicobar Island and Sombrero channel where internal tides are expected to be very strong show enhanced HN. Further, the HN is strong during spring tides as the tides are highly energetic during this period.

Data and Resources

The OBS data were acquired in the Andaman-Nicobar region under CSIR-GENIAS project. The waveform data for the HUTB station were provided by ESSO-INCOIS, Ministry of Earth Sciences, Govt. of India on 22nd August 2016. The tremometer code was used for automatic detection of harmonic noise (<https://github.com/dcroman/Tremometer>). The tidal currents were computed via TPXO web service (<https://tpxows.azurewebsites.net/> accessed on 11th Nov 2019).

Acknowledgments

We thank the Director, CSIR-NIO for supporting the study. We are grateful to the crew on board RV *Sindhu Sankalp* and the ship cell of CSIR-NIO for their assistance during the deployment and recovery operations of the OBSs on the cruises. We would like to thank the Director, ESSO-INCOIS for providing the HUTB data from ISLAND network. R. Reddy acknowledges the science and education research board (SERB) for national postdoctoral fellowship (NPDF). We thank all the reviewers and the associated editor for providing quality comments/suggestions which have improved the quality of the manuscript. The work was performed under the MLP1703 project of CSIR-NIO and the contribution no. is xxx.

References

- Alpers, W., H. Wang-Chen, and L. Hock (1997). Observations of internal waves in the Andaman Sea by ERS-SAR, Presented at *IEEE International Geoscience and Remote Sensing Symposium Proceedings. Remote Sensing-A Scientific Vision for Sustainable Development*. **4**, 1518–1520.
- Andersen, O. B. (1999). Shallow water tides in the northwest European shelf region from TOPEX/POSEIDON altimetry, *J. Geophys. Res.* **104**, no. C4, 7729–7741.
- Apel, J. R. (2002). Oceanic internal waves and solitons. In *An atlas of oceanic internal solitary waves*, Prepared for Office of Naval Research (Code 322 PO), 1–40.
- Ardhuin, F., L. Gualtieri, and E. Stutzmann (2015). How ocean waves rock the Earth: Two mechanisms explain microseisms with periods 3 to 300 s, *Geophys. Res. Lett.* **42**, no. 3, 765–772.
- Babcock, J. M., B. A. Kirkendall, and J. A. Orcutt (1994). Relationships between ocean bottom noise and the environment, *Bull. Seismol. Soc. Am.* **84**, no. 6, 1991–2007.
- Bromirski, P. D., F. K. Duennebieer, and R. A. Stephen (2005). Mid-ocean microseisms, *Geochem. Geophys. Geosys.* **6**, no. 4, doi: 10.1029/2004GC000768.
- Cacchione, D. A., and D. E. Drake (1986). Nepheloid layers and internal waves over continental shelves and slopes, *Geo-Marine Lett.* **6**, no. 3, 147–152.
- Cacchione, D. A., L. F. Pratson, and A. S. Ogston (2002). The Shaping of Continental Slopes by Internal Tides, *Science* **296**, no. 5568, 724–727.
- Cacchione, D., and L. Pratson (2004). Internal Tides and the Continental Slope, *Am. Sci.* **92**, no. 2, 130, doi:10.1511/2004.46.924.
- Chang, E. T. Y., B. F. Chao, G.-Y. Chen, and J.-M. Liao (2016). Internal tides recorded at ocean bottom off the coast of Southeast Taiwan, *J. Geophys. Res.* **121**, no. 5, 3381–3394.
- Cox, C. S., and D. C. Jacobs (1989). Cartesian diver observations of double frequency pressure-fluctuations in the upper levels of the ocean, *Geophys. Res. Lett.* **16**, no. 8, 807–810.
- Cox, C., T. Deaton, and S. Webb (1984). A deep-sea differential pressure gauge, *J. Atmos. Ocean Technol.* **1**, no. 3, 237–246.
- Crawford, W. C., and S. C. Webb (2000). Identifying and removing tilt noise from low-frequency (<0.1 Hz) seafloor vertical seismic data, *Bull. Seismol. Soc. Am.* **90**, no. 4, 952–963, doi:10.1785/0119990121.
- Curry, J. R. (2005). Tectonics and history of the Andaman Sea region, *J. Asian Earth Sci.* **25**, no. 1, 187–232, doi:10.1016/j.jseaes.2004.09.001.
- da Silva, J. C. B., and J. M. Magalhaes (2016). Internal solitons in the Andaman Sea: a new look at an old problem, in *Proceedings Remote Sens. Ocean, Sea Ice, Coast. Waters, Large Water Reg. SPIE 9999*, 999907. doi:10.1117/12.2241198.

- Dewangan, P., R. Reddy, K. A. Kamesh Raju, P. Singha, K. K. Aswini, V. Yatheesh, K. Samudrala, and M. Shuhail (2017). Nature of the Ambient Noise, Site Response, and Orientation of Ocean-Bottom Seismometers (OBSs): Scientific Results of a Passive Seismic Experiment in the Andaman Sea, *Bull. Seismol. Soc. Am.* **108**, no. 1, 248–259.
- Dickson, R. R., and I. N. McCave (1986). Nepheloid layers on the continental slope west of Porcupine Bank, *Deep Sea Res.* **33**, no. 6, 791–818.
- Doran, A. K., and G. Laske (2016). Infragravity waves and horizontal seafloor compliance, *J. Geophys. Res.* **121**, no. 1, 260–278.
- D'spain, G. L., W. S. Hodgkiss, and G. L. Edmonds (1991). The simultaneous measurement of infrasonic acoustic particle-velocity and acoustic pressure in the ocean by freely drifting Swallow floats, *IEEE J. Ocean Eng.* **16**, no. 2, 195–207.
- Duennebier, F. K., G. Blackinton, and G. H. Sutton (1981). Current-generated noise recorded on ocean bottom seismometers, *Mar. Geophys. Res.* **5**, no. 1, 109–115.
- Duennebier, F. K., P. N. Anderson, and G. J. Fryer (1987). Azimuth determination of and from horizontal ocean bottom seismic sensors, *Geophys. Res.* **92**, no. B5, 3567–3572.
- Dziak, R. P., and C. G. Fox (1999). The January 1998 earthquake swarm at axial volcano, Juan de Fuca Ridge: Hydroacoustic evidence of seafloor volcanic activity, *Geophys. Res. Lett.* **26**, no. 23, 3429–3432.
- Egbert, G.D., and S. Y. Erofeeva (2002). Efficient inverse modeling of barotropic ocean tides. *J. Atmos. Oceanic Technol.* **19**, no. 2, 183–204.
- Fox, C. G., and R. P. Dziak (1998). Hydroacoustic detection of volcanic activity on the Gorda Ridge, February-March 1996, *Deep Sea Res.* **45**, no. 12, 2513–2530.
- Franek, P., J. Mienert, S. Buenz, and L. Géli (2014). Character of seismic motion at a location of a gas hydrate-bearing mud volcano on the SW Barents Sea margin, *J. Geophys. Res.* **119**, no. 8, 6159–6177.
- Geissler, W. H., L. M. Matias, S. Monna, D. Stich, A. IbenBrahim, F. Mancilla, N. Zitellini, and NEAREST Working Group (2009). From Tides to Whale calls-Broadband ocean-bottom recordings from the Gulf of Cadiz, Presented at *EGU General Assembly Conference*, Abstract 5613.
- Geissler, W. H., L. Matias, D. Stich, F. Carrilho, W. Jokat, S. Monna, A. IbenBrahim, F. Mancilla, M.-A. Gutscher, V. Sallarès, and N. Zitellini (2010). Focal mechanisms for sub-crustal earthquakes in the Gulf of Cadiz from a dense OBS deployment, *Geophys. Res. Lett.* **37**, no. 18, 7–12.
- Gohl, K. (2010). The Expedition of the Research Vessel “Polarstern” to the Amundsen Sea, Antarctica, in 2010 (ANT-XXVI/3), *Berichtezur Polar-und Meeresforsch / Reports on Polar Mar. Res.* **617**, 173 pp., <http://epic.awi.de/29635/>
- Hannemann, K., F. Krüger, and T. Dahm (2013). Measuring of clock drift rates and static time offsets of ocean bottom stations by means of ambient noise, *Geophys. J. Int.* **196**, no. 2, 1034–1042.

- Hendershott, M. C. (1981). Long waves and ocean tides, in *Evolution of physical oceanography*, The MIT Press, 292-341.
- Hello, Y., A. Ogé, A. Sukhovich, and G. Nolet (2011). Modern mermaids: New floats image the deep Earth, *Eos Trans. AGU*.**92**, no. 40, 337–338.
- Holloway, P. E., and M. A. Merrifield (1999). Internal tide generation by seamounts, ridges, and islands, *J. Geophys. Res.* **104**, no. C11, 25937–25951.
- Hyder, P., D. R. G. Jeans, E. Cauquil, and R. Nerzic (2005). Observations and predictability of internal solitons in the northern Andaman Sea, *Appl. Ocean Res.***27**, no. 1, 1–11.
- Kamesh Raju, K. A., D. Ray, A. Mudholkar, G. P. S. Murty, V. K. Gahalaut, K. Samudrala, A. L. Paropkari, R. Ramachandran, and L. S. Prakash (2012). Tectonic and volcanic implications of a cratered seamount off Nicobar Island, Andaman Sea, *J. Asian Earth Sci.* **56**, 42–53, doi:10.1016/j.jseaes.2012.04.018.
- Konstantinou, K. I., and V. Schlindwein (2002). Nature, wavefield properties and source mechanism of volcanic tremor: A review, *J. Volcanol. Geotherm. Res.***119**, no. 4, 161–187, doi:10.1016/S0377-0273(02)00311-6.
- Lay, T., H. Kanamori, C. J. Ammon, M. Nettles, S. N. Ward, R. C. Aster, S. L. Bilek, M. R. Brudzinski, R. Butler, H. R. DeShon, G. Ekström, K. Satake, S. Sipkin (2005). The great Sumatra-Andaman earthquake of 26 December 2004, *Science***308**, no. 5725, 1127–1133.
- Longuet-Higgins, M. S. (1950). A theory of the origin of microseisms, *Phil.Trans. Roy. Soc. Lond.* **243**, no. 857, 1–35.
- Mohanty, S., A. D. Rao, and G. Latha (2018). Energetics of Semidiurnal Internal Tides in the Andaman Sea, *J. Geophys. Res.***123**, no. 9, 6224–6240.
- Munk, W. H. (1981). Internal waves and small-scale processes, in *Evolution of Physical Oceanography*, BA Warren and C. Wunsch (Editors). MIT Press, Cambridge, 264–291.
- Murty, T. S., and R. F. Henry (1983). Tides in the Bay of Bengal, *J. Geophys. Res.***88**, no. C10, 6069–6076.
- Olofsson, B. (2010). Marine ambient seismic noise in the frequency range 1-10 Hz, *The Leading Edge***29**, no. 4, 418–435.
- Osborne, A. R., and T. L. Burch (1980). Internal Solitons in the Andaman Sea, *Science***208**, 451–460.
- Perry, R. B., and G. R. Schimke (1965). Large-amplitude internal waves observed off the northwest coast of Sumatra, *J. Geophys. Res.***70**, no. 10, 2319–2324.
- Pomar, L., M. Morsilli, P. Hallock, and B. Bádenas (2012). Internal waves, an under-explored source of turbulence events in the sedimentary record, *Earth-Science Rev.***111**, 56–81.
- Pontoise, B., and Y. Hello (2002). Monochromatic infra-sound waves recorded offshore Ecuador: Possible evidence of methane release, *Terra Nov.***14**, no. 6, 425–435.

- Puig, P., A. Palanques, J. Guillén, and M. El Khatab (2004). Role of internal waves in the generation of nepheloid layers on the northwestern Alboran slope: Implications for continental margin shaping, *J. Geophys. Res.* **109**, no. C9, 1–11.
- Quaresma, L. S., J. Vitorino, A. Oliveira, and J. da Silva (2007). Evidence of sediment resuspension by nonlinear internal waves on the western Portuguese mid-shelf, *Mar. Geol.* **246**, 123–143.
- Reiche, S., C. Hübscher, S. Brenner, C. Betzler, and J. K. Hall (2018). The role of internal waves in the late Quaternary evolution of the Israeli continental slope, *Mar. Geol.* **406**, 177–192.
- Rios, C., T. Dahm, and M. Jegen (2010). Using pressure and seismological broadband ocean data to model shear wave velocities in the north Atlantic, Presented at *EGU General Assembly Conference*, Abstracts 10518.
- Roman, D. C. (2017). Automated detection and characterization of harmonic tremor in continuous seismic data, *Geophys. Res. Lett.* **44**, no. 12, 6065–6073, doi:10.1002/2017GL073715.
- Romanowicz, B. (1991). Seismic tomography of the Earth's mantle, *Annu. Rev. Earth Planet. Sci.* **19**, no. 1, 77–99.
- Sarma, V. V. S. S., and P. V Narvekar (2001). A study on inorganic carbon components in the Andaman Sea during the post monsoon season, *Oceanol. Acta.* **24**, no. 2, 125–134.
- Shepard, F.P., N. F. Marshall, P. A. Mcloughlin, G. G. Sullivan (1979). Currents in submarine canyons and other sea valleys. *Studies in Geology* Am. Assoc. Pet. Geol. vol., Tulsa, 173 pp.
- Simons, F. J., G. Nolet, P. Georgief, J. M. Babcock, L. A. Regier, and R. E. Davis (2009). On the potential of recording earthquakes for global seismic tomography by low-cost autonomous instruments in the oceans, *J. Geophys. Res.* **114**, no. B5, 1–16.
- Singha, P., P. Dewangan, K. A. Kamesh Raju, K. K. Aswini and T. R. Reddy (2019). Geometry of the Subducting Indian Plate and Local Seismicity in the Andaman Region from the Passive OBS Experiment, *Bull. Seismol. Soc. Am.* **109**, no. 2, 797–811.
- Stähler, S. C. (2016). Performance report of the RHUM-RUM ocean bottom seismometer network around La Réunion, western Indian Ocean, *Adv. Geosci.* **41**, 43–63.
- Stähler, S. C., M. C. Schmidt-Aursch, G. Hein, and R. Mars (2018). A Self-Noise Model for the German DEPAS OBS Pool, *Seismol. Res. Lett.* **89**, no. 5, 1838–1845.
- Thomson, R. E., S. E. Roth, and J. Dymond (1990). Near-inertial motions over a mid-ocean ridge: Effects of topography and hydrothermal plumes, *J. Geophys. Res.* **95**, no. C5, 7261–7278.
- Tolstoy, M., S. Constable, J. Orcutt, H. Staudigel, F. K. Wyatt, and G. Anderson (1998). Short and long baseline tiltmeter measurements on axial seamount, Juan de Fuca Ridge, *Phys. earth Planet. Inter.* **108**, no. 2, 129–141.
- Trehu, A. M. (1985). A note on the effect of bottom currents on an ocean bottom seismometer, *Bull. Seismol. Soc. Am.* **75**, no. 4, 1195–1204.

- Ugalde, A., B. Gaithe, M. Ruiz, A. Villaseñor, and C. R. Ranero (2019). Seismicity and Noise Recorded by Passive Seismic Monitoring of Drilling Operations Offshore the Eastern Canary Islands, *Seismol. Res. Lett.* **90**, no. 4, 1565-1576, doi: 10.1785/0220180353.
- Webb, S. C. (1998). Broadband seismology and noise under the ocean, *Rev. Geophys.* **36**, no. 1, 105–142, doi:10.1029/97RG02287.
- Webb, S. C. (2007). The Earth’s “hum” is driven by ocean waves over the continental shelves, *Nature* **445**, no. 7129, 754–756.
- Webb, S. C., and C. S. Cox (1986). Observations and modeling of seafloor microseisms, *J. Geophys. Res.* **91**, no. B7, 7343–7358.
- Webb, S. C., and W. C. Crawford (1999). Long-period seafloor seismology and deformation under ocean waves, *Bull. Seismol. Soc. Am.* **89**, no. 6, 1535–1542.
- Wenz, G. M. (1962). Acoustic ambient noise in the ocean: Spectra and sources, *J. Acoust. Soc. Am.* **34**, no. 12, 1936–1956.
- Wyssession, M. E. (1996). How well do we utilize global seismicity?, *Bull. Seismol. Soc. Am.* **86**, no. 5, 1207-1219.
- Xie, X., Q. Liu, and Z. Zhao (2018). Deep Sea Currents Driven by Breaking Internal Tides on the Continental Slope, *Geophys. Res. Lett.* **45**, no. 12, 6160–6166.

The full mailing address for each author

Ramakrushana Reddy. T (Postdoctoral Fellow)
CSIR-National Institute of Oceanography (NIO), Goa
Email: ramareddy@nio.org

Pawan Dewangan (Senior Scientist)
CSIR-National Institute of Oceanography (NIO), Goa
Email: pdewangan@nio.org

Lalit Arya (Intern Student)
CSIR-National Institute of Oceanography (NIO), Goa
Email: alalit@nio.org

PabitraSingha (Ph.D. Scholar)
CSIR-National Institute of Oceanography (NIO), Goa
Email: psingha@nio.org

Kamesh Raju K.A (Chief Scientist)
CSIR-National Institute of Oceanography (NIO), Goa
Email: kameshraj@gmail.com

List of figure captions

Figure 1. Satellite-derived bathymetry map showing the location of OBS stations deployed in the Andaman-Nicobar region. The star and the number represent the location and name of OBS station, respectively. The diamond represents the land station (HUTB). The inset shows the study area in the Bay of Bengal.

Figure 2. Raw one-hour data of the vertical (a), horizontals (b, e) and pressure (f) components at OBS02. Their spectrograms are shown in panels c, d, g, and h, respectively. The spectrograms show sharp spectral peaks which are characterized by a fundamental frequency and several overtones occurring at integer multiples of the fundamental frequency.

Figure 3. Hourly count of HN estimated at all OBS stations (OBS01 to OBS12). The HN is observed for the entire deployment period, however, the duration of the HN varies considerably among the stations. A broad low-frequency fluctuation with a periodicity of ~ 15 days is observed which is superimposed by a high-frequency fluctuation with multiple periodicities ranging from ~ 6 to ~ 12 hr. The solid vertical line indicates the transition from previous month to next month.

Figure 4. Hourly count of HN for vertical, horizontals and pressure components at OBS02. Z represents the vertical component, H1 and H2 represent the horizontal components and P represents the pressure component. The HN is continuously observed for the vertical and horizontals components, but is less frequent for the pressure component.

Figure 5. Spectral analysis of the hourly count of HN estimated from the vertical component of OBS01, OBS02, OBS09, and OBS11. Several distinct peaks which correspond to the lunar and solar tidal periodicities are observed. The fortnightly periodicity (Mf) is clearly observed at the OBS stations. The two principal semi-diurnal tidal constituents due to the moon and sun (M2 and S2) with periods of 12.42 hr and 12.00 hr are also observed. Further, we also observed compound tides (2MS2, 2SM2, and MS4) and overtones (M4 and M6) for most of the OBS stations. The insets show the enlarged view of the tidal periodicities.

Figure 6. a) Photograph of the DEPAS OBS instrument showing head buoy, seismometers, hydrophone, and other peripheral units. b) Schematic representation of DEPAS OBS on deployment.

Figure 7. a) MODIS reflectance imagery data from the Aqua satellite (<https://worldview.earthdata.nasa.gov/>) on 21st March 2014 in the Andaman-Nicobar region. The internal tides are marked in the image using solid arrow while the cloud covers are marked with dashed arrow. The zoom-out image illustrating the internal tides is shown at all OBS stations. b) The result from Massachusetts Institute of Technology general circulation model (MITgcm) highlighting the generation sites for the internal tides (solid striped boxes), and propagation of energy flux (represented by arrows) in the Andaman-Nicobar region (modified after Mohanty *et al.*, 2018). AI is the Andaman Islands; LA is the Little Andaman Island; CN is the Car Nicobar Island; NI is the Nicobar Islands.

Figure 8. (a) Comparison between daily count of HN from OBS02 and estimated peak envelop of total tidal current at OBS02. b) Same as Figure 8a but for OBS09. The HN occurs preferentially during spring tides and are almost absent during neap tides. The solid vertical line indicates the transition from previous month to next month.

List of Tables

OBS Station	Total duration of HN (in hours)	Depth (m)	Total duration of HN (expressed as % of deployment period)
OBS01	205.35	3900	7.13
OBS02	543.93	1832	18.89
OBS03	4.7	4183	0.16
OBS05	14.3	1969	0.49
OBS06	24.7	3439	0.86
OBS07	28.95	3611	1.01
OBS09	258.25	2264	8.97
OBS11	335.28	1650	11.64
OBS12	15.3	3485	0.53

Table 1: Total duration of HN estimated from the vertical component of the OBS stations.

Figure 1

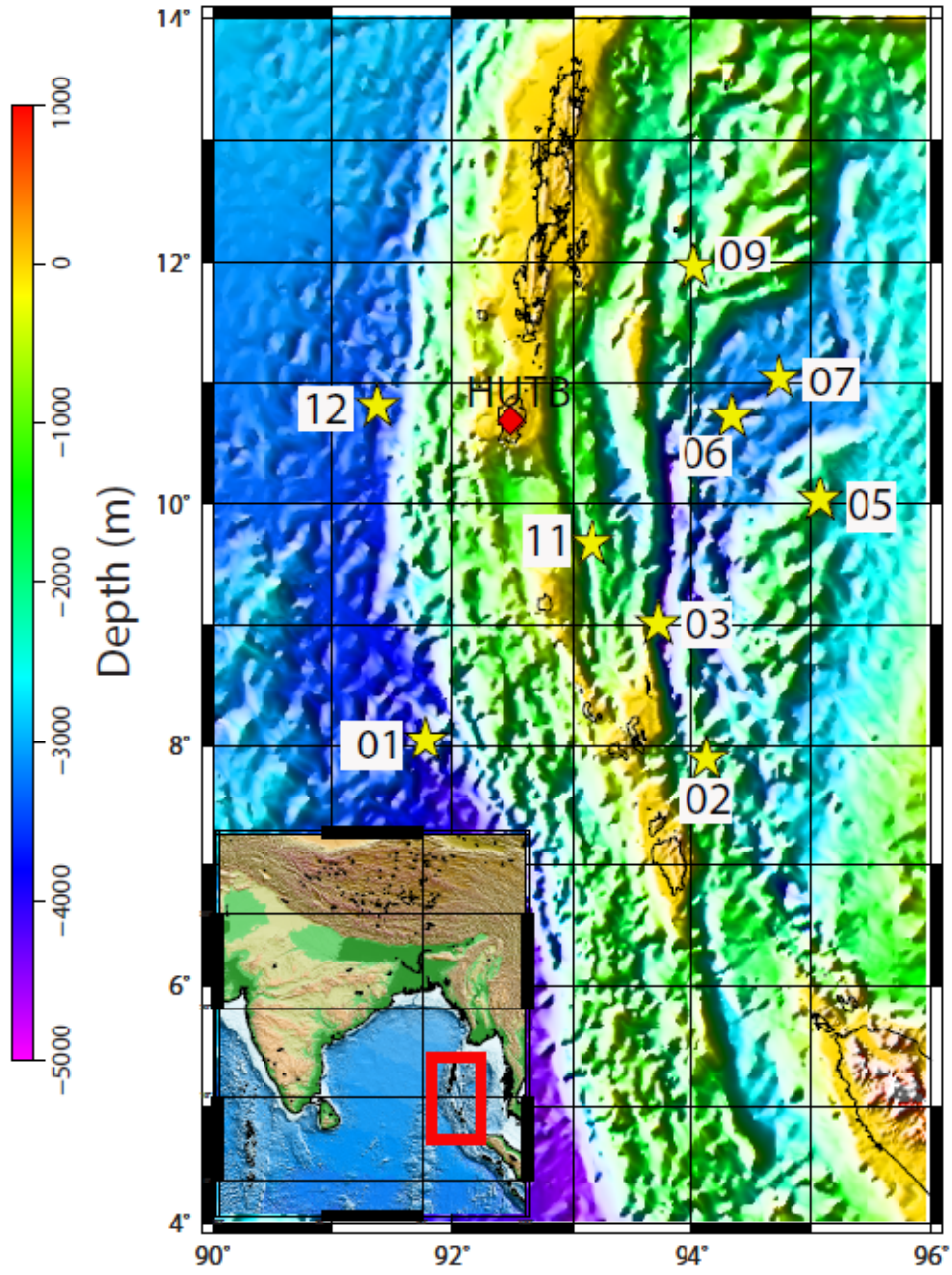


Figure 2

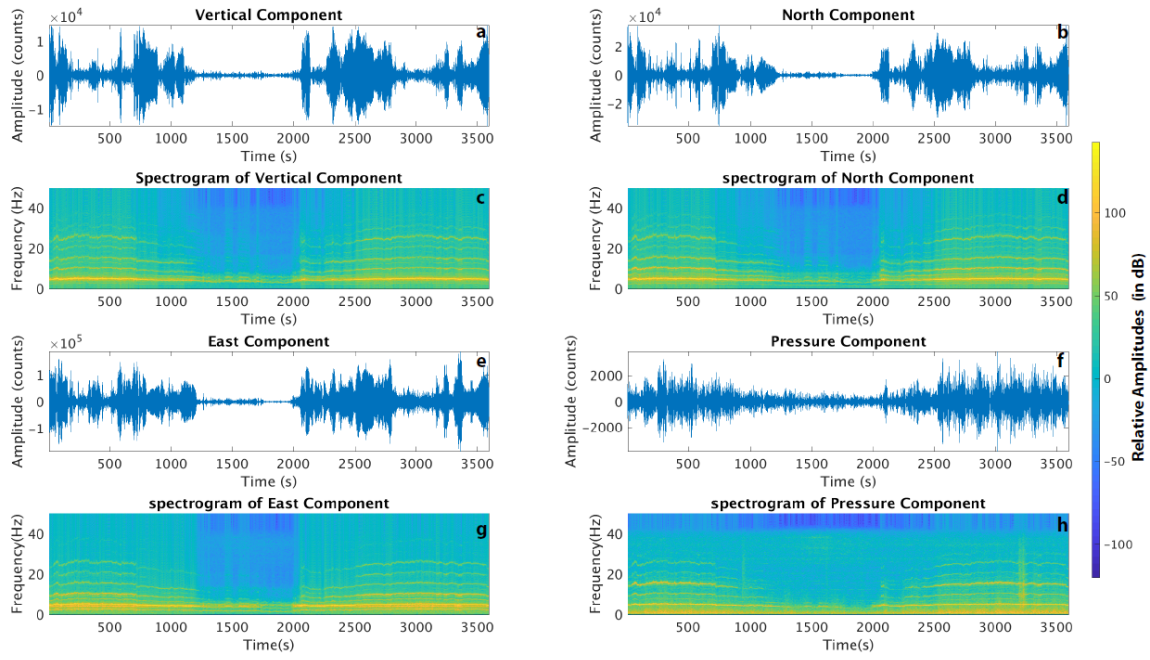


Figure 3

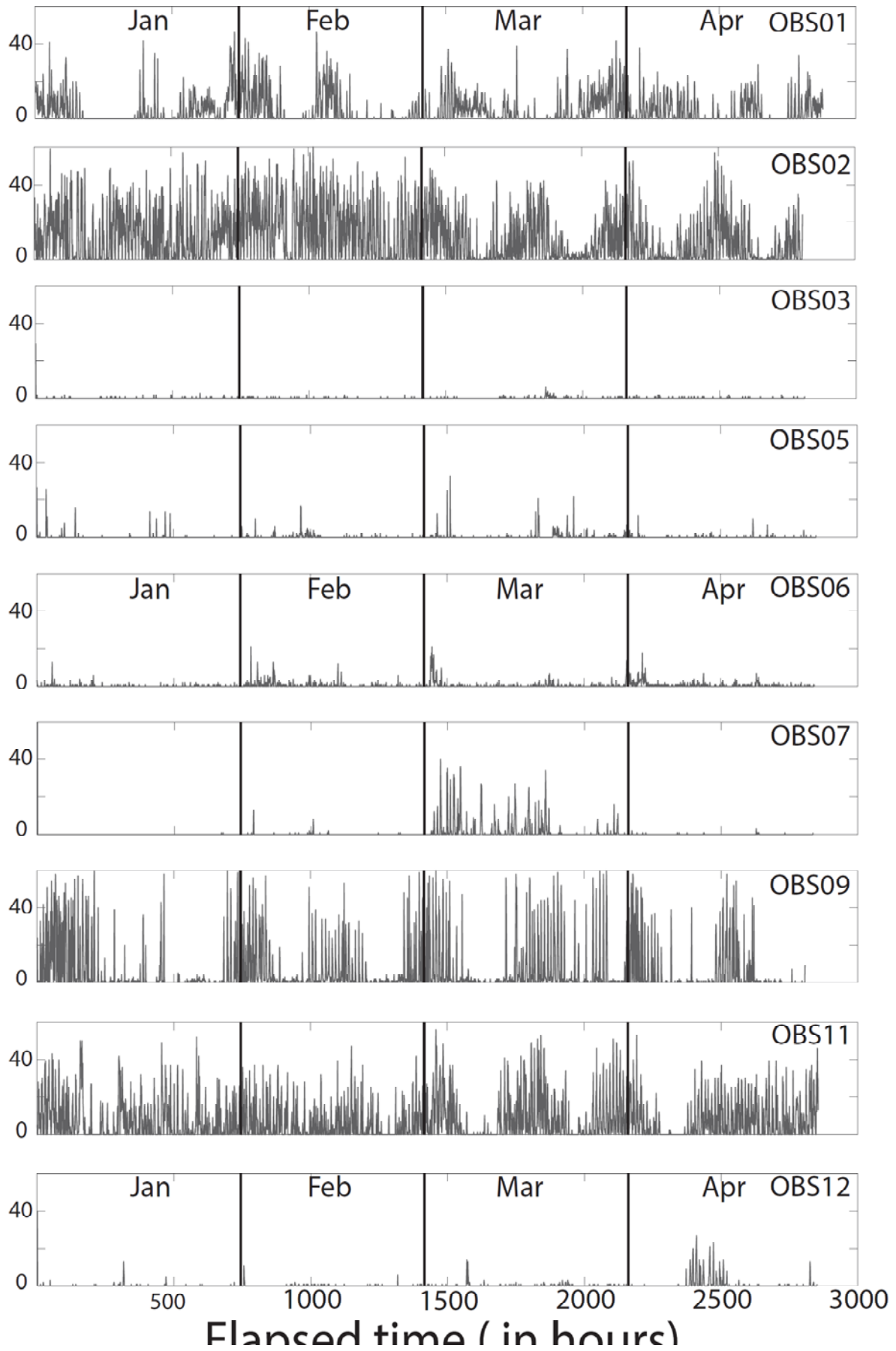


Figure 4

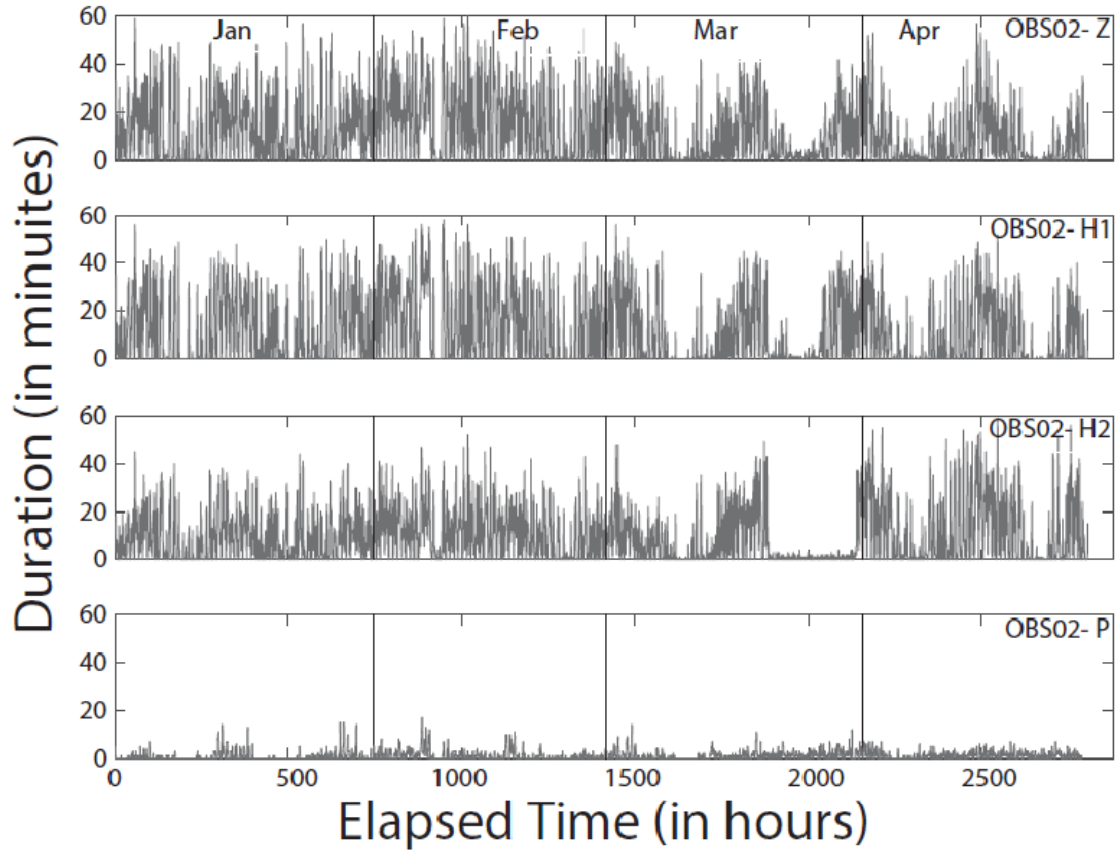


Figure 5

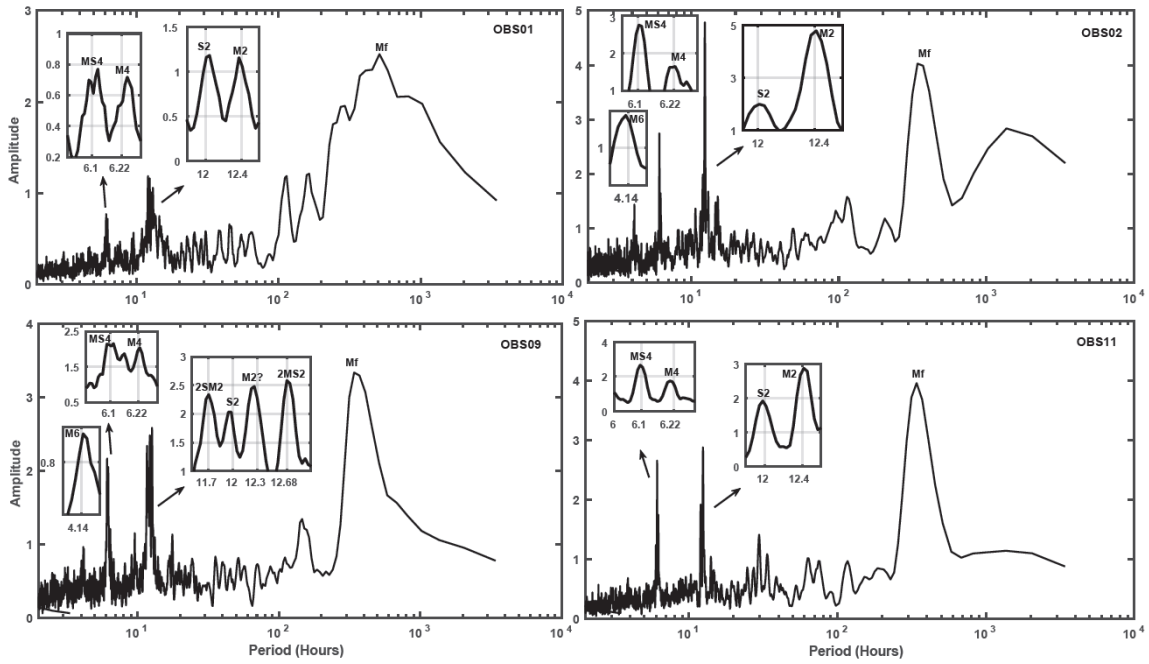


Figure 6

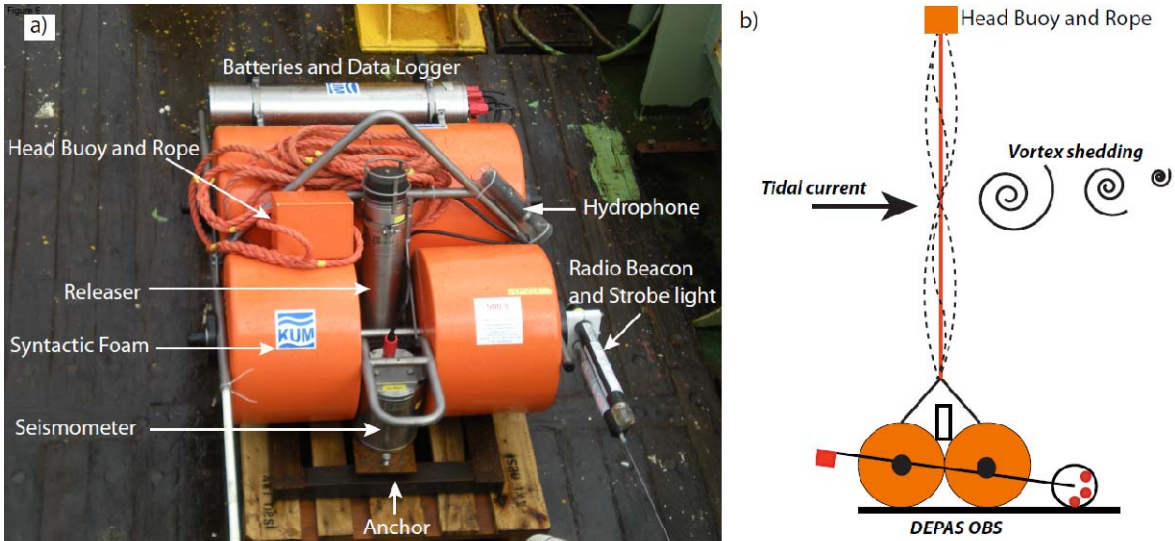


Figure 7a

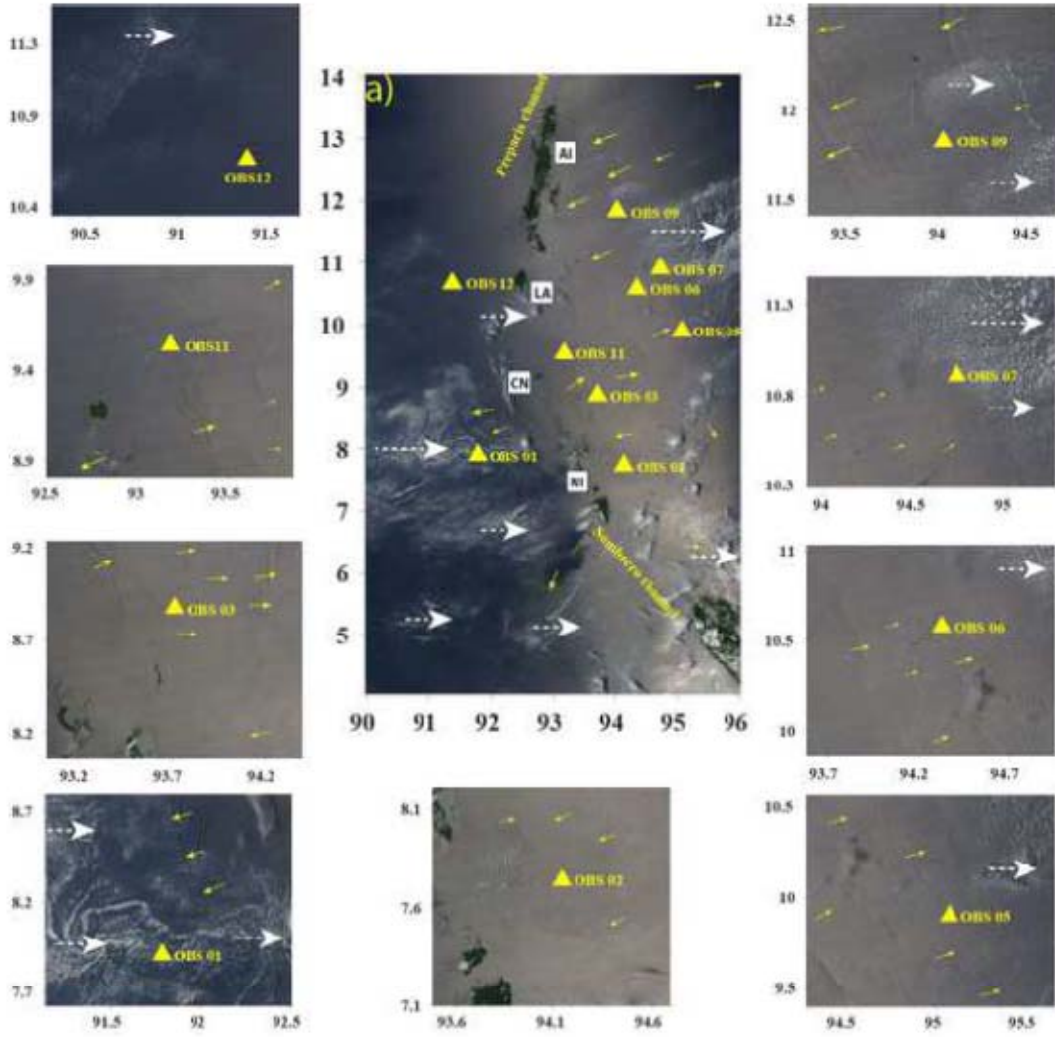


Figure 7b

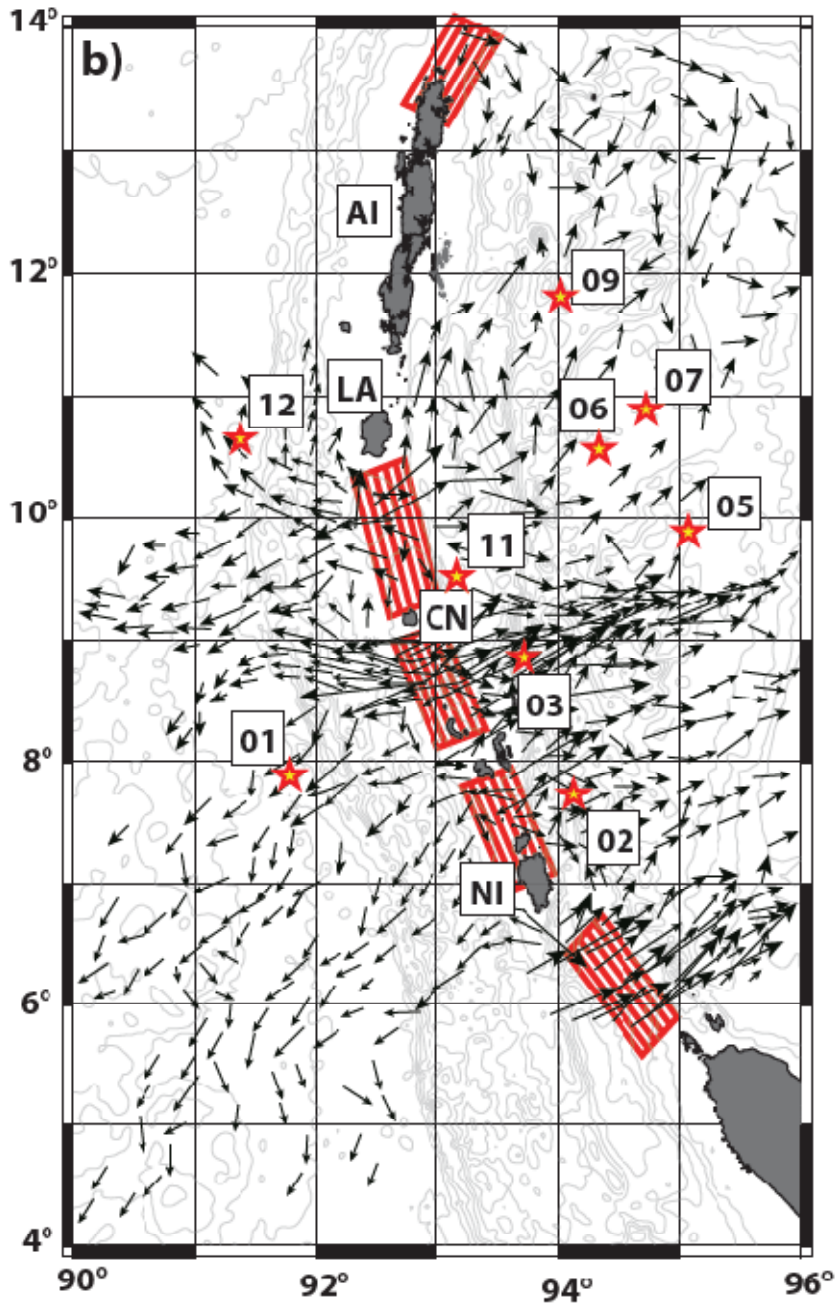


Figure 8

